Int. J. Heat Mass Transfer. Vol. 37, No. 2, pp. 229–236, 1994
Printed in Great Britain

0017–9310/94 $6.00 + 0.00

Conjugate free convection due to a vertical plate in a porous medium

MICHAEL VYNNYCKY and SHIGEO KIMURA
Government Industrial Research Institute, Tohoku, Agency of Industrial Science and Technology, Ministry of International Trade and Industry, Nigatake, 4-2-1, Miyagino-Ku, Sendai, 983, Japan

(*Received* 19 *April* 1993 *and in final form* 8 *July* 1993)

Abstract—Two-dimensional conjugate free convection due to a vertical plate of finite extent adjacent to a semi-infinite porous medium is investigated numerically using finite-difference techniques. Computed solutions to the governing heat and momentum equations are obtained for a wide range of different values of the non-dimensional parameters that are present in the problem, namely the Rayleigh number, Ra, the thermal conductivity ratio, k, between the plate and the porous medium, and the plate aspect ratio, λ. The results give good agreement with results obtained by other authors for k, $Ra \gg 1$, and compare very favourably with an approximate analytical one-dimensional analogue which is developed for $Ra \gg 1$.

1. INTRODUCTION

THE PROBLEM of natural convection due to a heated vertical plate embedded in a fluid-saturated porous medium is of considerable practical and fundamental interest. Heat transfer from a heated vertical plate provides probably one of the most basic scenarios for natural convection problems. Variations of the problem occur frequently in the literature (see, for example, Ingham and Brown [1], Cheng and Pop [2]), although to the best of the authors' knowledge there have been only a few works which deal with conduction–convection conjugate effects. Perhaps the most important contributions in this field were made by Bejan and Anderson [3, 4] who looked at the conjugate nature of heat transfer within a configuration where a conductive impermeable partition separates two fluid reservoirs which are at different temperatures; even there, however, the analysis was limited to the case of a thin plate. Furthermore, investigations in the literature relating to conjugate effects in other geometries are not abundant either; for example, convection from a horizontal cylinder in an infinite fluid or fluid-saturated porous medium has only recently been studied by Kimura and Pop [5, 6]. It is, therefore, the dearth of work in this subject which provides the motivation for this paper.

In what follows, in Section 2 we provide a mathematical formulation of the steady-state problem, and write down the appropriate non-dimensional governing equations. In Section 3, we indicate a simple one-dimensional analogue for the 2-d equations in Section 2. In Sections 4 and 5, with the aid of a numerical solution to the two-dimensional momentum and heat equations, we are able to predict theoretically the flow and temperature distributions in the solid and the porous medium; in addition, we demonstrate the effect of key non-dimensional parameters on the problem, namely the Rayleigh number, the ratio of the thermal conductivities of the solid and porous medium and the aspect ratio of the solid plate, and show how the present problem reduces to that of a heated vertical plate considered by Cheng and Minkowycz [7]. Also, we demonstrate the good agreement between the full computations and the 1-d analogue of Section 3. Conclusions are drawn in Section 6.

2. MATHEMATICAL FORMULATION

Consider the steady free convection flow due to a rectangular plate occupying the region $-a \leqslant x \leqslant 0$, $-(b/2) \leqslant y \leqslant (b/2)$, adjacent to a semi-infinite fluid-saturated porous medium ($x > 0$, $-\infty \leqslant y \leqslant \infty$) at temperature T_∞ (Fig. 1). The left-hand side of the plate is held at a uniform temperature T_c ($> T_\infty$), whilst the sides $y = \pm(b/2)$ are insulated; for the porous medium, there is no heat flux and no normal outflow across $x = 0$, $|y| > (b/2)$. For $x = 0$, $|y| < (b/2)$, we expect both continuity of temperature and heat flux; in addition, we assume that the porous medium is isotropic and homogeneous and that the fluid is incompressible. Invoking the Boussinesq–Darcy approximation, the free convection flow is described by the equations of continuity

$$\frac{\partial u}{\partial x} + \frac{\partial v}{\partial y} = 0 \tag{1}$$

and momentum

$$\frac{\partial u}{\partial y} - \frac{\partial v}{\partial x} = -\frac{g\beta K}{\nu}\frac{\partial T_f}{\partial x}, \tag{2}$$

the equation of energy in the fluid–porous medium

$$u\frac{\partial T_f}{\partial x} + v\frac{\partial T_f}{\partial y} = \alpha\left(\frac{\partial^2 T_f}{\partial x^2} + \frac{\partial^2 T_f}{\partial y^2}\right) \tag{3}$$

and the equation of heat transfer inside the solid plate

NOMENCLATURE

a	thickness of the conducting plate
b	length of the conducting plate
g	acceleration due to gravity
k_f	effective thermal conductivity of the porous medium
k_s	thermal conductivity of the plate
k	thermal conductivity ratio, k_s/k_f
K	permeability of the porous medium
M_1^s	total number of grid points in the x-direction in conducting plate
M_2^s	total number of grid points in the y-direction in conducting plate
M_1^f	total number of grid points in the x-direction in porous medium
M_2^f	total number of grid points in the y-direction in porous medium
Ra	Rayleigh number for the porous medium, $Kg\beta(T_c-T_\infty)b/\alpha\nu$
$\bar{T}_b$	dimensionless average boundary temperature, $(T_b-T_c)/(T_c-T_\infty)$
T_c	constant temperature of heated side of plate
T_∞	constant temperature of ambient fluid
u, v	dimensionless velocity components along (x, y) axes
x	horizontal coordinate
X_∞	size of computational domain in x-direction
y	vertical coordinate
Y_∞	size of computational domain in y-direction.

Greek symbols

α	thermal diffusivity
β	coefficient of thermal expansion
δ	boundary layer thickness
$\Delta\theta$	temperature increment
$\Delta\psi$	streamline increment
θ_s	dimensionless temperature in the solid
θ_f	dimensionless temperature in the porous medium
λ	aspect ratio, a/b
ν	kinematic viscosity
ψ	dimensionless streamfunction.

$$\frac{\partial^2 T_s}{\partial x^2}+\frac{\partial^2 T_s}{\partial y^2}=0, \tag{4}$$

where (u, v) are the velocity components in the (x, y) directions, T_f and T_s are the temperatures of the fluid-saturated porous medium and the solid plate respectively, and the physical constants g, β, ν, K, α (and later k_s and k_f) are as given in the table of nomenclature. Equations (1)–(4) are subject to the following boundary conditions:

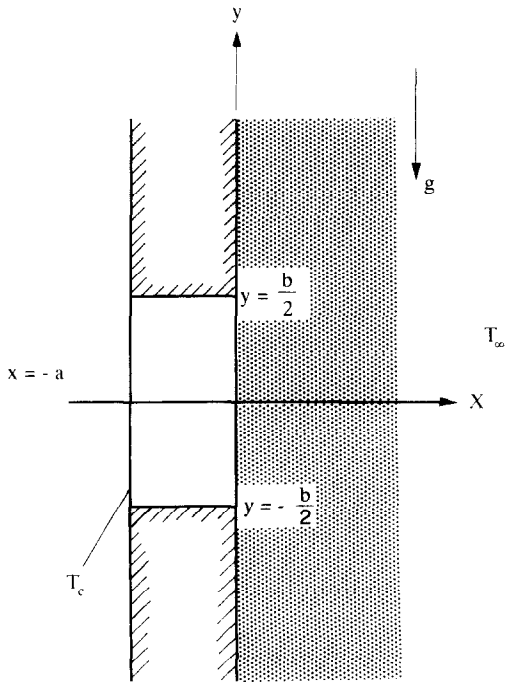

FIG. 1. Sketch of geometry for natural convection.

$$u=0 \quad \text{on} \quad x=0, \tag{5}$$

$$T_s=T_f,\ k_f\frac{\partial T_f}{\partial x}=k_s\frac{\partial T_s}{\partial x} \quad \text{on} \quad x=0,\ |y|\leqslant\frac{b}{2}, \tag{6}$$

$$\frac{\partial T_f}{\partial x}=0 \quad \text{on} \quad x=0,\ |y|>\frac{b}{2}, \tag{7}$$

$$T_s=T_c \quad \text{on} \quad x=-a,\ |y|\leqslant\frac{b}{2}, \tag{8}$$

$$\frac{\partial T_s}{\partial y}=0 \quad \text{on} \quad y=\pm\frac{b}{2},\ -a\leqslant x\leqslant 0, \tag{9}$$

$$T_f\to T_\infty \quad \text{as} \quad x\to\infty,\ y\to\pm\infty, \tag{10}$$

$$v\to 0 \quad \text{as} \quad x\to\infty, \tag{11}$$

$$u\to 0 \quad \text{as} \quad y\to\pm\infty. \tag{12}$$

By employing the following nondimensionalisation,

$$x^*=\frac{x}{b},\quad y^*=\frac{y}{b},\quad u^*=\frac{bu}{\alpha},\quad v^*=\frac{bv}{\alpha},$$

$$\theta_s^*=\frac{T_s-T_\infty}{T_c-T_\infty},\quad \theta_f^*=\frac{T_f-T_\infty}{T_c-T_\infty}$$

subsequently dropping the asterisks and then defining the dimensionless streamfunction by

$$u = \frac{\partial \psi}{\partial y}, \quad v = -\frac{\partial \psi}{\partial x},$$

we arrive at the following system of dimensionless equations for momentum and heat transfer, respectively, in the porous medium,

$$\nabla^2 \psi = -Ra \frac{\partial \theta_f}{\partial x}, \tag{13}$$

$$u \frac{\partial \theta_f}{\partial x} + v \frac{\partial \theta_f}{\partial y} = \nabla^2 \theta_f, \tag{14}$$

where ψ and θ_f are the dimensionless streamfunction and temperature, respectively; also, $Ra = g\beta K b(T_c - T_\infty)/\alpha\nu$ is the Rayleigh number for the fluid–porous medium and ∇^2 denotes the two-dimensional Laplacian. In addition we have the equation of heat transfer in the solid,

$$\nabla^2 \theta_s = 0, \tag{15}$$

where θ_s denotes the dimensionless temperature in the solid. Equations (13)–(15) are now subject to the nondimensional form of the boundary conditions (5)–(12), that is

$$\psi = 0 \quad \text{on} \quad x = 0, \tag{16}$$

$$\theta_s = \theta_f, \; k \frac{\partial \theta_f}{\partial x} = \frac{\partial \theta_s}{\partial x} \quad \text{on} \quad x = 0, \; |y| \leqslant \frac{1}{2}, \tag{17}$$

$$\frac{\partial \theta_f}{\partial x} = 0 \quad \text{on} \quad x = 0, \; |y| > \frac{1}{2}, \tag{18}$$

$$\theta_s = 1 \quad \text{on} \quad x = -\lambda, \; |y| \leqslant \frac{1}{2}, \tag{19}$$

$$\frac{\partial \theta_s}{\partial y} = 0 \quad \text{on} \quad y = \pm \frac{1}{2}, \; -\lambda \leqslant x \leqslant 0, \tag{20}$$

$$\theta_f \to 0 \quad \text{as} \quad x \to \infty, \; y \to \pm\infty, \tag{21}$$

$$\frac{\partial \psi}{\partial x} \to 0 \quad \text{as} \quad x \to \infty, \tag{22}$$

$$\frac{\partial \psi}{\partial y} \to 0 \quad \text{as} \quad y \to \pm\infty, \tag{23}$$

where $\lambda = a/b$ denotes the aspect ratio of the conducting plate and $k = k_s/k_f$ is the ratio of the thermal conductivities in the conducting solid and the porous medium. The physical quantities which are then of most interest are the dimensionless local Nusselt number, given by

$$Nu = -\left(\frac{\partial \theta_f}{\partial x}\right)_{x=0}, \quad |y| \leqslant \frac{1}{2},$$

and the dimensionless average Nusselt number, given by

$$\overline{Nu} = \int_{-(1/2)}^{1/2} Nu \, dy.$$

3. APPROXIMATE ANALYTICAL SOLUTION

Before proceeding with a numerical solution to equations (13)–(23), it is useful to consider first an approximate one-dimensional solution to the conjugate heat transfer problem; this may be done for $Ra \gg 1$ by considering the heat balance between the solid and fluid interface ($x = 0, |y| \leqslant (b/2)$). The heat flux per unit area q'' may be expressed as

$$q'' = k_s \frac{(T_c - T_b)}{a} = k_f \frac{(T_b - T_\infty)}{\delta}, \tag{24}$$

where T_b is the average temperature at the interface, defined by

$$T_b = \frac{1}{b} \int_{-(b/2)}^{b/2} T(0, y) \, dy$$

and δ is the thickness of the boundary layer along the interface which is given by

$$\frac{\delta}{b} = 1.126 Ra^{*-(1/2)}, \tag{25}$$

where the last equation has been obtained using (see Cheng and Minkowycz [7])

$$\overline{Nu} = 0.888 Ra^{*1/2}, \tag{26}$$

with Ra^* as the actual Rayleigh number, based on $(T_b - T_\infty)$. In addition, noting that the apparent Rayleigh number, Ra, whch is based on the temperature difference $(T_c - T_\infty)$ in the conjugate problem, is related to the actual Rayleigh number, by $Ra^* = Ra\bar{T}_b$, where we have defined $\bar{T}_b = (T_b - T_\infty)/(T_c - T_\infty)$, we may combine (24) and (25) to obtain

$$F(X) \equiv \mu X^3 + X^2 - 1 = 0, \tag{27}$$

where $X = \sqrt{(T_b)}$ and $\mu \; (= \lambda Ra^{1/2}/1.126k > 0)$ is analogous to the Biot number which often occurs in conduction studies (see, for example, Bejan [8]). It is then straightforward to derive that (27) has only one real root if $\mu > (2/\sqrt{27})$, two real roots if $\mu = 2/\sqrt{27}$ and three real roots if $\mu < (2/\sqrt{27})$. For the second and third cases, it is clear that, since $F'(X) = 0$ when $X = 0, \; -(2/3\mu)$ and $F(-1) = -\mu \; (<0)$, there is a unique solution for $\bar{T}_b$ such that $0 \leqslant \bar{T}_b \leqslant 1$; hence there is a unique solution for $\bar{T}_b$ for all values of μ, which may be shown to lie in the interval [0, 1] and derived to be

$$\bar{T}_b = \begin{cases} \dfrac{1}{9\mu^2}\left((\gamma + \sqrt{(\gamma^2 - 1)})^{1/3} + (\gamma + \sqrt{(\gamma^2 - 1)})^{-1/3} - 1\right)^2 & \text{if } \mu > \dfrac{2}{\sqrt{27}}, \\ \dfrac{\sqrt{3}}{2} & \text{if } \mu = \dfrac{2}{\sqrt{27}}, \\ \dfrac{1}{9\mu^2}\left(2\cos\left(\dfrac{1}{3}\cos^{-1}(\gamma)\right) - 1\right)^2 & \text{if } \mu < \dfrac{2}{\sqrt{27}}, \end{cases} \tag{28}$$

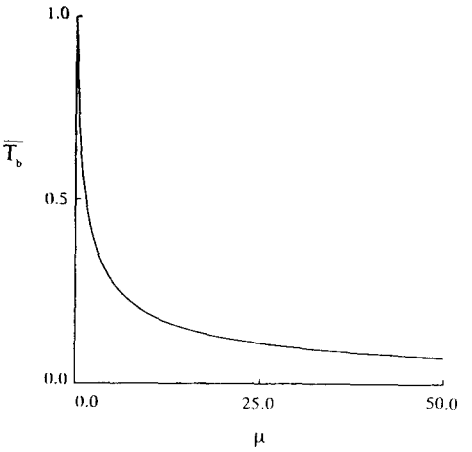

FIG. 2. Solution to equation (28) for $\bar{T}_b$ as a function of μ.

where $\gamma = (27\mu^2/2) - 1$. The solution for $\bar{T}_b$ as a function of μ is plotted in Fig. 2, and will be compared later with the numerical computations of Sections 4 and 5.

Further, from the definition of the average Nusselt number ($\overline{Nu}$) in terms of T_b, we have

$$\overline{Nu} = \frac{q''a}{k_f(T_c - T_\infty)} \sim \frac{T_b - T_\infty}{T_c - T_\infty} Ra^{*1/2} = \bar{T}_b^{3/2} Ra^{1/2}, \tag{29}$$

which suggests that

$$\frac{\overline{Nu}}{\bar{T}_b^{3/2} Ra^{1/2}} = \text{constant}. \tag{30}$$

Although we have no means of determining this constant exactly, the aim is to try different values to see which one best fits the numerical results to be obtained in Section 5; ultimately, in fact, a value of 0.9 was deemed suitable.

Despite the *ad hoc* nature of this analytical approach, several points are worthy of note. First, from an engineering perspective, equations (28) and (29) are useful because they provide closed-form expressions for $\bar{T}_b$ and $\overline{Nu}$ in terms of the other parameters in the problem, most notably the apparent Rayleigh number, based on the prescribed temperature difference between the heated plate and the porous medium, as opposed to the a priori indeterminable actual Rayleigh number. Second, from an analytical viewpoint, it is worth noting that for all values of Ra, k and λ, the cubic equation (27) leads to a unique solution for $\bar{T}_b$, as one would expect on physical grounds.

4. NUMERICAL SOLUTION

The partial differential equations (13)–(15) were finite-differenced using a control volume approach and non-uniform grid network as described by Patankar [9]. Initially, 5000 nodal points were used for the discretisation of the porous medium (50 in the x-direction and 100 in the y-direction), whilst for the solid plate, 400 nodal points (20 in both x and y directions) were employed. One difficulty, however, was to determine and to implement numerically the far field boundary conditions (21)–(23). In order to allow for the anticipated development of a thermal plume near $x = 0$ as $y \to \infty$, it was decided instead to use open boundary conditions given by

$$\theta_f = 0 \text{ if } u < 0 \text{ at } x = X_\infty,$$

$$\frac{\partial \theta_f}{\partial x} = 0 \text{ if } u > 0 \text{ at } x = X_\infty,$$

$$\theta_f = 0 \text{ if } v < 0 \text{ at } y = Y_\infty,$$

$$\frac{\partial \theta_f}{\partial y} = 0 \text{ if } v > 0 \text{ at } y = Y_\infty,$$

$$\theta_f = 0 \text{ if } v > 0 \text{ at } y = -Y_\infty,$$

$$\frac{\partial \theta_f}{\partial y} = 0 \text{ if } v < 0 \text{ at } y = -Y_\infty,$$

$$\frac{\partial \psi}{\partial x} = 0 \text{ at } x = X_\infty,$$

$$\frac{\partial \psi}{\partial y} = 0 \text{ at } y = \pm Y_\infty,$$

where the constants X_∞ and Y_∞ were varied between 2 and 10, in order to determine the effect of computational domain size on the solution. This is demonstrated in Fig. 3, where $\overline{Nu}/Ra^{1/2}$ is plotted against X_∞ ($= Y_\infty$) with $k = 1000$ and $Ra = 1000$. In particular, we observe that the difference between the values of $\overline{Nu}/Ra^{1/2}$ for $X_\infty = 5$ and 10 is of the order of a few per cent; however, in view of the saving in terms of computing time which accrues by using $X_\infty = 5$ instead of $X_\infty = 10$, coupled with not too great a loss in terms of accuracy, subsequent calculations were carried out using the former value. The code was tested further by keeping $k = 1000$, and varying Ra; in this case, we expect that, for large values of Ra, the results for the local Nusselt number at the conjugate boundary should approach those of Cheng and Minkowycz [7] for natural convection due to an infinitely long isothermal plate adjacent to a porous medium. That this was indeed the case is shown in Fig. 4, where the quantity $Nu/Ra^{1/2}$ is plotted against length along the plate for different values of the Rayleigh number. In addition, in Fig. 5 we demonstrate the effect of

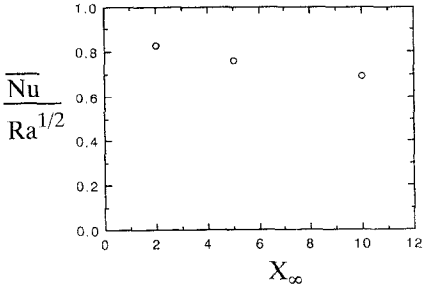

FIG. 3. ($Nu/Ra^{1/2}$) vs size of computational domain (X_∞).

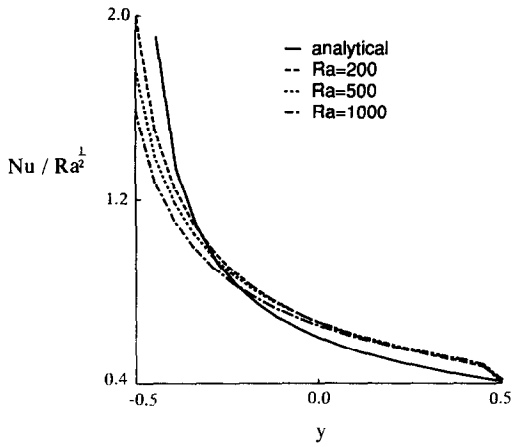

FIG. 4. $(Nu/Ra^{1/2})$ vs distance along plate (y) $(k = 1000)$.

the open boundary conditions discussed earlier. The figure shows the streamline and isotherm plots (streamlines on the left) for the entire computational domain for the case when $k = 1$, $\lambda = 1$ and $Ra = 800$, and illustrates that the open boundary conditions approximate adequately to the actual physical boundary conditions posed by equations (10)–(12).

Each of the above computations, however, required approximately 10 h of CPU time on a Titan Workstation, so it was decided to carry out subsequent computations for $\lambda = 1$ using $M_1^s = M_2^s = 10$, $M_1^f = 25$, $M_2^f = 50$; for different values of λ, M_1^s and M_2^s were altered in such a way as to keep the mesh spacing in both x and y directions in the solid at most 0.1. In all cases, a refined mesh was used adjacent to the conjugate boundary in order to take account accurately of the boundary conditions given by (17). Since the numerical scheme employed was very similar to that used by Kimura and Pop [5], we omit further details, except to mention that the convergence criterion used for the termination of the computation was

$$\frac{\sum_{i}^{M_1^f}\sum_{j}^{M_2^f}|\theta_{f_{ij}}^{n+1}-\theta_{f_{ij}}^{n}|}{\sum_{i}^{M_1^f}\sum_{j}^{M_2^f}|\theta_{f_{ij}}^{n}|} < 10^{-6},$$

where the superscript n denotes the iteration order. Instead, we move on to a presentation of the results, computed for $X_\infty = Y_\infty = 5$ and for a wide range of values of the parameters k, λ and Ra.

5. RESULTS

Detailed streamline and isotherm behaviour are shown in Figs. 6–8 for $k = 1$ and 10, $\lambda = 0.25$ and 1, and $Ra = 50$ and 800; in each figure, the left-hand plot represents the streamline pattern, the right-hand one the isotherm pattern. As might have been expected, thermal plumes, whose widths decrease with increasing Rayleigh number, are seen to develop near the top edge of the plate; in addition, a thermal boundary layer is seen to develop at the conjugate boundary. Furthermore, as k is increased, the thermal resistance of the solid plate is reduced, resulting in a much stronger buoyancy force on the fluid–porous medium; a similar effect is also obtained by decreasing the value of the aspect ratio, λ. Comparing the isotherms for $\lambda = 0.25$ (Fig. 8) and $\lambda = 1$ (Fig. 7), one may observe that the thermal resistivity in the latter case is around half that for the former, a result which is somewhat different from that which one might expect from an analogy with a simple conduction problem involving two adjacent plates, one of thickness λ

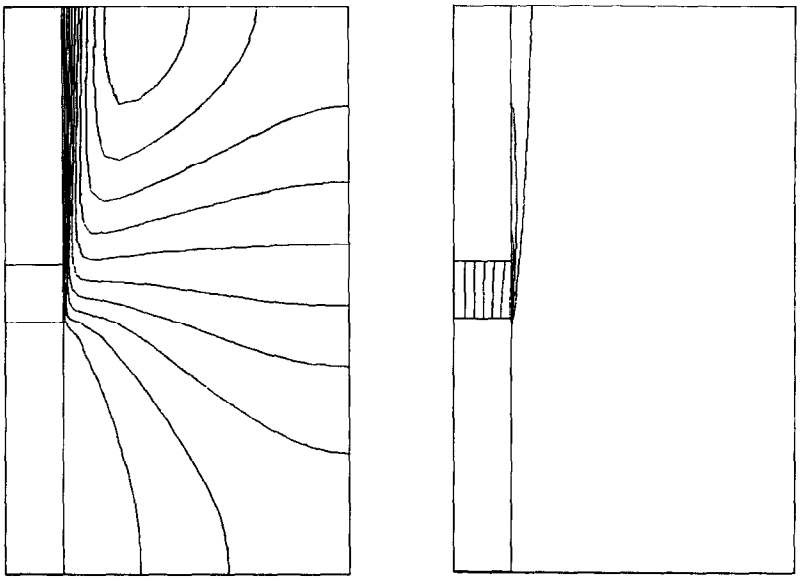

FIG. 5. Streamlines and isotherms for $k = 1$, $\lambda = 1$ and $Ra = 800$ ($\Delta\psi = 5$ and $\Delta\theta = 0.1$).

whose left-hand end is at unit temperature, the other of thickness δ whose right-hand end is at zero temperature; in this case, simple analysis shows that the boundary between the two plates attains a temperature

$$\bar{T}_b = \frac{1}{1 + \frac{\lambda}{k\delta}},$$

and thence that for the case when $k\delta \ll 1$, the boundary temperature is roughly four times greater when $\lambda = 0.25$ than when $\lambda = 1$. This provides a good example of the complications that arise because of conjugate effects: the thermal resistivity within the vertical plate does not decrease in proportion to a reduction in its thickness, because the reduced resistivity in the plate causes an increase in convective heat transfer in the porous medium, which thereby reduces the thermal resistivity on the porous side of the conjugate boundary also.

Figures 9 and 10 show the variation of temperature and local Nusselt number, respectively, at the conjugate boundary for $k = 2.5$, $\lambda = 1$ and $Ra = 50$ and 800. These plots are quite typical of the results obtained for relatively low values of the parameter k, and indicate the essentially linear behaviour of the temperature with distance along the plate; this effect is seen to a lesser extent for the Nusselt number, owing to the discontinuities in the flux at the endpoints of the plate, although the profile is nevertheless linear along the plate's central portion. For higher values of k, such as those used in obtaining the results in Fig. 4, one may, however, expect a departure from linearity. The variations of the average temperature and the average Nusselt number at the conjugate boundary for different values of Ra, k and λ are shown in Figs. 11 and 12. In particular, the computed results have been compared with those obtained using equation (28) from Section 3; as was mentioned in that section, the choice of 0.9 as the constant of proportionality resulting from equation (30) leads to very good agreement between analytical and computed results for a wide range of parameter values. As regards the boundary temperature, however, one may observe that at the lowest value of the Rayleigh number ($Ra = 50$), there is an apparent difference between the analytical and numerical predictions for some parameter sets (for example, $k = 2.5$ and 10, $\lambda = 1$); in retrospect, this is not too surprising since a boundary-layer approximation was used in developing equation (28). Nonetheless, the overall agreement may be deemed extremely good if one considers the complexity of the problem and the simplicity of the analysis. As regards the mean Nusselt number, it is clear that this becomes less dependent on the Rayleigh number as the thermal conductivity ratio, k, decreases;

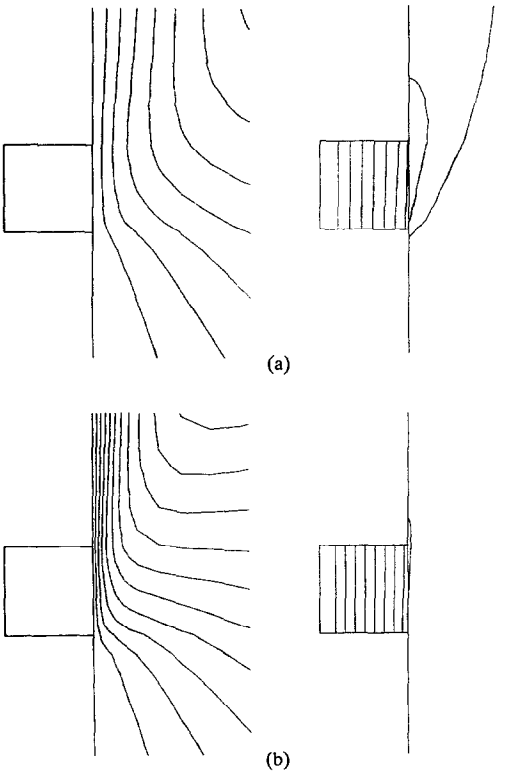

FIG. 6. Streamlines and isotherms for $k = 1$ and $\lambda = 1$: (a) $Ra = 50$, $\Delta\psi = 1$ and $\Delta\theta = 0.1$; (b) $Ra = 800$, $\Delta\psi = 2$ and $\Delta\theta = 0.1$.

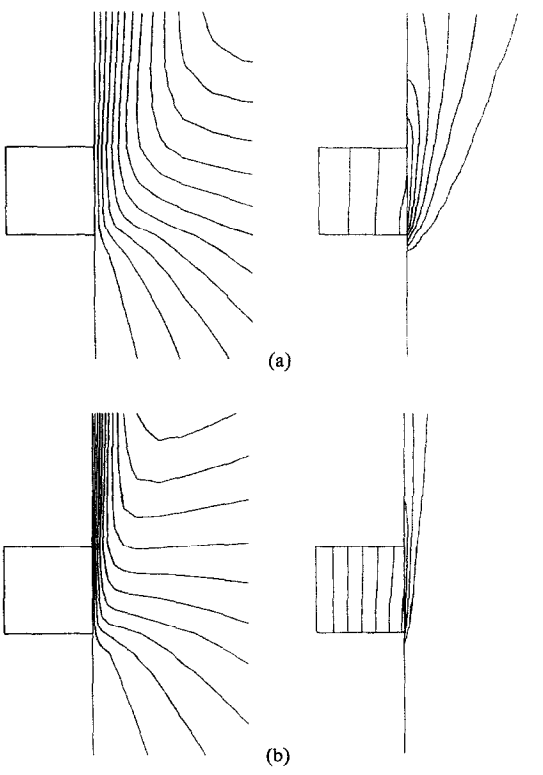

FIG. 7. Streamlines and isotherms for $k = 10$ and $\lambda = 1$: (a) $Ra = 50$, $\Delta\psi = 1$ and $\Delta\theta = 0.1$; (b) $Ra = 800$, $\Delta\psi = 4$ and $\Delta\theta = 0.1$.

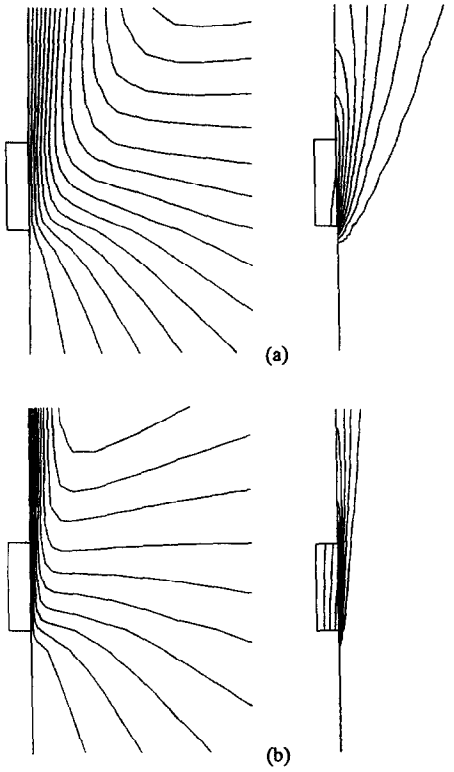

FIG. 8. Streamlines and isotherms for $k = 10$ and $\lambda = 0.25$: (a) $Ra = 50$, $\Delta\psi = 1$ and $\Delta\theta = 0.1$; (b) $Ra = 800$, $\Delta\psi = 5$ and $\Delta\theta = 0.1$.

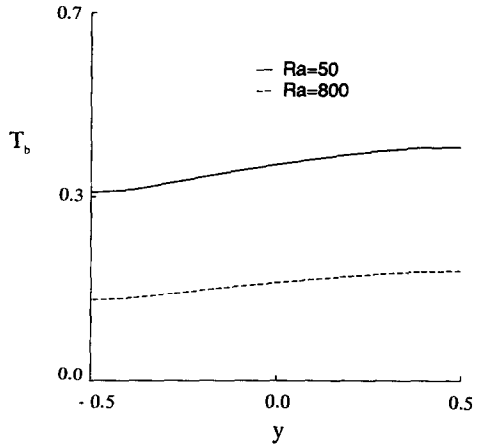

FIG. 9. Boundary temperature (T_b) vs distance along plate (y) ($k = 2.5$, $Ra = 50$ and 800).

within the presently investigated parameter range, the mean Nusselt number is essentially independent of the Rayleigh number when $k < 2.5$ and $Ra > 200$ for $\lambda = 1$, and when $k < 1$ and $Ra > 200$ for $\lambda = 0.25$.

6. CONCLUSION

This investigation has considered the problem of conjugate free convection due to a vertical plate adjacent to a semi-infinite porous medium. By solving the

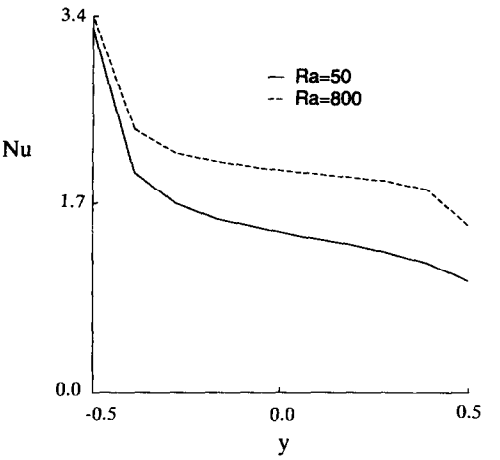

FIG. 10. Local Nusselt number (Nu) vs distance along plate (y) ($k = 2.5$, $Ra = 50$ and 800).

heat and transfer equations numerically using finite-difference techniques, it has been possible to provide a detailed description of the effect of non-dimensional parameters such as the Rayleigh number, the ratio of the thermal conductivities and the plate aspect ratio on the flow and heat transfer characteristics. For high Rayleigh numbers, an approximate analytical approach was possible, the results of which were sub-

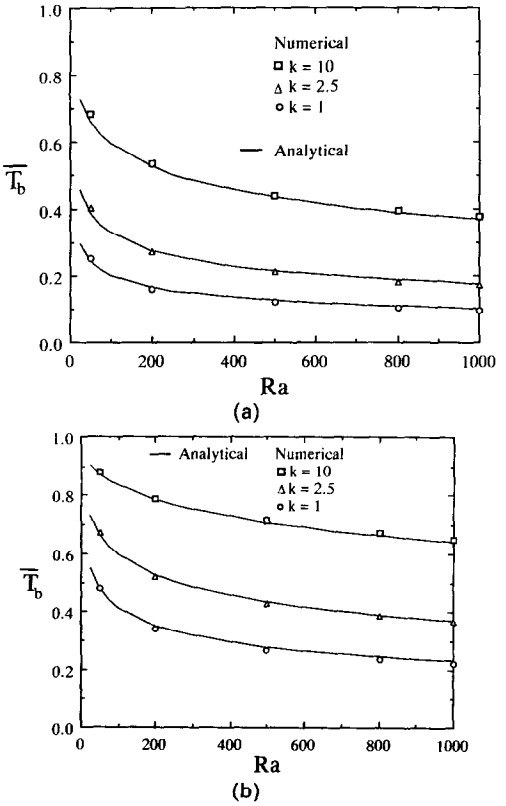

FIG. 11. Average boundary temperature ($\bar{T}_b$) vs Rayleigh number (Ra) for $k = 1$, 2.5 and 10: (a) $\lambda = 1$; (b) $\lambda = 0.25$.

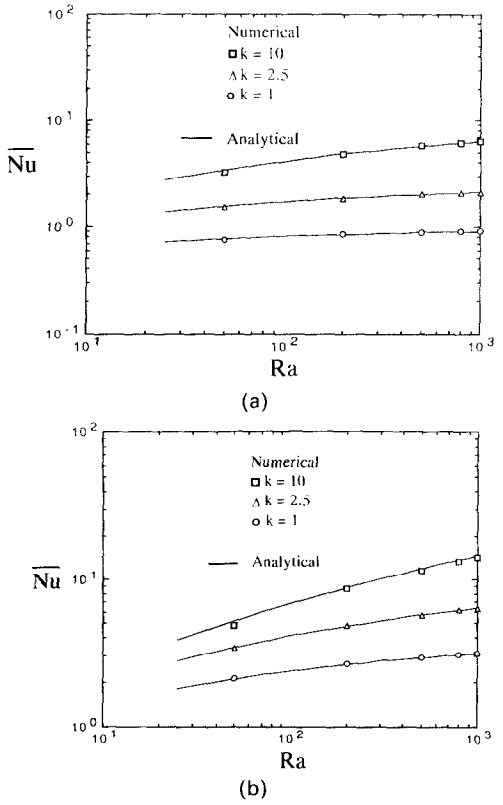

FIG. 12. Average Nusselt number ($\overline{Nu}$) vs Rayleigh number (Ra) for $k = 1$, 2.5 and 10: (a) $\lambda = 1$; $\lambda = 0.25$.

sequently seen to compare favourably with the full numerical computations. The analytical solution, although *ad hoc* in nature, does have several advantages over the fully-computed solution: it is very compact, it predicts satisfactorily the average temperature and Nusselt number at the conjugate boundary for a wide range of values of Ra, k and λ and requires negligible computing time. Overall, therefore, the dual analytical and computational approach adopted in this paper is thought to provide a comprehensive account of steady-state conjugate free convection induced by a heated vertical plate.

REFERENCES

1. D. B. Ingham and S. N. Brown, Flow past a suddenly heated vertical plate in a porous medium, *Proc. Roy. Soc. London Ser. A* **403,** 51–80 (1986).
2. P. Cheng and I. Pop, Transient free convection about a vertical flat plate imbedded in a porous medium, *Int. J. Engng Sci.* **22,** 253–264 (1984).
3. A. Bejan and R. Anderson, Heat transfer across a vertical impermeable partition imbedded in a porous medium, *Int. J. Heat Mass Transfer* **24,** 1237–1245 (1981).
4. A. Bejan and R. Anderson, Natural convection at the interface between a vertical porous layer and an open space, *ASME J. Heat Transfer* **105,** 124–129 (1983).
5. S. Kimura and I. Pop, Conjugate free convection from a circular cylinder in a porous medium, *Int. J. Heat Mass Transfer* **85,** 3105–3113 (1992).
6. S. Kimura and I. Pop, Conjugate natural convection from a horizontal cylinder, *Numer. Heat Transfer*, accepted for publication.
7. P. Cheng and W. J. Minkowycz, Free convection about a vertical flat plate embedded in a porous medium with application to heat transfer from a dike, *J. Geophys. Res.* **82,** 2040–2044 (1977).
8. A. Bejan, *Convective Heat Transfer*. Wiley, New York (1984).
9. S. V. Patankar, *Numerical Heat Transfer and Fluid Flow*. Hemisphere, New York (1980).